Talanta 217 (2020) 121012

Contents lists available at ScienceDirect

Talanta

journal homepage: www.elsevier.com/locate/talanta

Quantitative imaging of structured complex metal oxide thin films using online-LASIL-ICP-MS

C. Herzig[a], J. Frank[b], A.K. Opitz[a], J. Fleig[a], A. Limbeck[a,*]

[a] TU Wien, Institute of Chemical Technologies and Analytics, Vienna, Austria
[b] TU Wien, Joint Workshop, Technical Chemistry, Vienna, Austria

ARTICLE INFO

Keywords:
Online-laser ablation of solids in liquid (online-LASIL)
Geometrically structured thin films
Quantified 2D-mapping
Online-quantification approach

ABSTRACT

Online-laser ablation of solids in liquid (online-LASIL) coupled with ICP-MS detection was used as a new sampling strategy for the analysis of complex metal oxide (CMO) thin films. The in-house built and optimized online-LASIL ablation cell provides the unique possibility to correlate the signal intensities with the spatial origin of the signal at the sample. For that purpose a particle transport with as little particle dispersion as possible is crucial. To demonstrate the 2D imaging capability of this technique, geometrically structured samples with varying composition were prepared by pulsed laser deposition (PLD) and ion beam etching procedures. These thin films with a thickness of 220 nm were spatially resolved analysed. As a result, 2D intensity maps obtained by online-LASIL can be reported for the first time. Additionally a new approach for simultaneous online quantification was developed by adopting the standard addition concept allowing to correct for instrumental drifts of long time measurements.

1. Introduction

Laser ablation of solid materials submerged into a liquid – commonly referred to as laser ablation in liquid (LAL) or laser ablation of solids/samples in liquid (LASIL) – is gaining more and more attention since the beginning of the 1990s. This can be explained by the two main purposes of applying this technique: (i) production of nanoparticles and (ii) the use as a new sampling strategy of solid materials prior to inorganic element analysis.

The field of laser induced nanoparticle production is very rich in different applications beginning in 1993 when Neddersen et al. produced Au nanoparticles, which were used for surface enhanced Raman spectroscopy [1]. These nanoparticles were produced by placing an Au target in a liquid and focusing a laser beam onto the surface of the metal. Since then, a great effort was put on understanding the physical principles of nanoparticle formation by laser ablation in liquid [2–4] and how these findings can be applied to develop preparation methods for different target materials [5]. Nanoparticle generation *via* this LASIL route is not restricted to certain materials. The production of nanoparticles based on metals [6], semiconductors [7] or ceramics [8] is well reported in literature. Until now, the process efficiency can be increased up to several grams of nanoparticles per hour [9]. The possibilities of influencing the size and shape of the particles even allow the synthesis of hollow nanoparticles of metal oxides [10] or quantum dots of SnO_2 [11] or SiC [12].

The second branch of the LASIL community is not interested in the properties of the produced nanoparticles, but uses the generated nanoparticle suspension to draw analytical conclusions about the solid target material. In this approach, the target is an unknown solid sample and LASIL is employed as a novel sampling method. This idea was proposed by Muravitskaya et al. [13] for the first time in 2009 and several materials, for example metal alloys [13], glasses (e.g. NIST 610/611)[14, 15] and ceramics (SiC [16], GaN [17]) were investigated by this method until now, confirming the applicability of this concept.

The reason for this interest in a new solid sampling method can be explained by the drawbacks of the conventional approaches for the elemental analysis of solid samples. Solid sampling techniques, such as laser ablation – inductively coupled plasma – mass spectrometry (LA-ICP-MS) or – optical emission spectroscopy (LA-ICP-OES) require matrix matched standards due to matrix effects in the ablation, transportation and ionisation steps [18]. Unfortunately, those matrix matched standards are limited and for novel materials commercially unavailable. The alternative of in-house preparation and characterisation of standards is laborious and time consuming and thus for quite some cases too costly. In contrast, for liquid samples certified reference materials are easily commercially available and offer a high flexibility to fit the sample in composition and concentration. For this reason, a common approach is to transform the solid sample into a clear liquid – e.g. by

* Corresponding author. TU Wien, Institute of Chemical Technologies and Analytics, Getreidemarkt 9/164 I²AC, 1060, Vienna, Austria.
E-mail address: andreas.limbeck@tuwien.ac.at (A. Limbeck).

https://doi.org/10.1016/j.talanta.2020.121012
Received 5 February 2020; Received in revised form 2 April 2020; Accepted 6 April 2020
Available online 18 April 2020

dissolution or digestions techniques. However, these processes can sometimes be challenging and often require hazardous agents (e.g. hydrofluoric acid), additional equipment (e.g. microwave assisted digestion system) or further chemicals for fusions (lithium or sodium borate). Additionally the information about sample homogeneity is lost and only bulk information is obtained.

The attractiveness of using LASIL as an ICP sampling method for solids arises from the fact that it allows combining the advantages of liquid sampling and laser ablation while eliminating their disadvantages. Laser ablation in liquid media offers the possibility to directly convert the solid sample into a nanoparticle suspension. Subsequent conventional liquid analysis can be performed using liquid reference materials for signal quantification of such nanoparticle suspensions.

Recently we reported an online-LASIL approach [19], which allows the direct analysis of the nanoparticle suspension without any manual handling step between particle generation and analysis, as it is usually applied in literature. This handling step hampers ambitions towards automatization of the analysis and furthermore gives only access to average values of a bulk sample. For this reason, we developed and optimized an in-house built ablation cell, which is continuously flushed by a carrier solution to transport the nanoparticles produced at the cell directly to the liquid sample introduction system of an ICP-OES device. With this setup accurate and precise quantification of homogeneous thin films (ranging from 220 nm to 14 nm) of complex metal oxides could be demonstrated [20]. The great advantage of such an online-LASIL setup is that it gives access to further benefits of conventional solid sampling like obtaining laterally resolved information (2D mapping) and depth profiles. A key element for that purpose is an optimized ablation cell, which ensures short washout times and prevents particle dispersion.

The focus of the present work is to demonstrate the current capabilities of our online LASIL-system for obtaining spatially resolved information. For this aim, micro-patterned Gd-doped CeO_2 thin films with two different Gd cation contents (10 and 20 cation fraction cf%) were prepared. The films were grown by pulsed laser deposition (PLD) and circular structures were fabricated using photolithography in combination with Ar-ion beam etching. These structured thin films were analysed by online LASIL in combination with ICP-MS detection and 2D intensity maps were obtained. Additionally, correct stoichiometry maps were generated by quantifying the intensity signals using an adopted online standard addition concept with liquid standard solutions.

2. Experimental

2.1. LASIL-ICP instrumentation

Thin film analysis was carried out using a commercially available laser ablation system (New Wave 213, ESI, Freemont, CA) for particle generation. Since the absolute amount of an analyte is limited in imaging experiments with high lateral resolution (spot size 20 μm, 220 nm film thickness), ICP-MS (iCAP QC, ThermoFisher Scientific, Bremen, Germany) was used as detection system due to its high sensitivity and fast data acquisition. The ICP-MS instrument was tuned on a daily basis to ensure high sensitivity and valid data. Therefore, a tuning solution provided by the manufacturer was used and instrument parameters were chosen to obtain a maximum of ^{115}In signal, keep the oxide ratio of $^{140}Ce^{16}O/^{140}Ce$ below 2% and the amount of doubly charged ions ($^{138}Ba^{++}/^{138}Ba^{+}$) below 3%. Further details on measurement parameters can be found in Table 1.

The in-house produced ablation cell consists of a polyether-ether-ketone (PEEK) polymer body, a cavity for housing the sample with a geometry of $5 \times 5 \times 0.5\ mm^3$, two drillings for the in- and outlet of the carrier solution and the cover glass with a polymer foil (PDMS) for sealing. Detailed information about the cell design can be found elsewhere [20]. Carrier solution was transported in a PFA tube (0.25 mm ID) by a peristaltic pump (Perimax 12, SPETEC, Erding, Germany) to the liquid sample introduction system consisting of a concentric PFA nebulizer and a cyclonic spray chamber.

Table 1
Measurement parameters; Parameters marked with an asterisk used for imaging if several values given.

Laser ablation system	
Wavelength	213 nm
Pulse duration	4 ns
Repetition rate	20 Hz
Laser fluence	1.6 J cm^{-2}
Spot size	20 μm (intensity image) 25 μm (quantified image)
Scan speed	20 μm s^{-1}
ICP-MS detection system	
Cool gas flow	14 L min^{-1}
Auxiliary gas flow	0.65 L min^{-1}
Nebulizer gas flow	1.03 L min^{-1}
RF power	1550 W
Dwell time	1, 2, 3, 5, 10, 20, 30, 50* ms
Measured isotopes	^{138}Ce,^{140}Ce,^{142}Ce*,^{155}Gd,^{157}Gd,^{160}Gd*

2.2. Sample preparation

Gadolinium doped CeO_2 (GDC) thin films were chosen as an application example due to the wide chemical resistance and the importance of this CMO in the use of solid oxide fuel cells as an electrolyte or electrode. For thin film preparation an in-house built pulsed laser deposition system equipped with a KrF excimer laser (248 nm wavelength, Lambda COMPexPro 201F), a heater and a vacuum chamber was used. The laser was operated at a repetition rate of 5 Hz, 50 ns pulse duration and 400 mJ per pulse leading to approximately 1.5 J cm^{-2} laser fluence at the surface of the target. The target itself was prepared from commercially available GDC powder (Treibacher Industrie AG, Althofen, Austria) by isostatic pressing (ca. 2 kbar) and sintering at 1300 °C. Two targets with either 10 cf% Gd (GDC10) or 20 cf% Gd (GDC20) were used. As substrates, yttria stabilised zirconium dioxide single crystals (YSZ, 9.5 mol% Y_2O_3) with a size of $5 \times 5\ mm^2$ and 0.5 mm thickness (Crystec GmbH, Germany) were used. During the PLD process, an O_2-partial pressure of 0.04 mbar was adjusted, and the substrates were heated to 600 °C (measured by a pyrometer) to ensure crystalline film growth. 4800 laser pulses corresponding to 16 min of ablation time were necessary to obtain 220 nm thin films. The film thickness was determined with a profilometer (DektakXT, Bruker, Massachusetts, USA).

For micro-patterning of the GDC films photolithography and Ar-ion beam etching procedures were applied. Two types of geometrically structured samples were prepared – for a graphical illustration see Fig. 1. Sample type 1 shows circles with varying diameters consisting of GDC20. The area around the circles is solely bare YSZ substrate without any GDC20. The preparation process started with a plain GDC20 thin film on a YSZ substrate prepared by a PLD process, afterwards a structured polymer overlay with circles of different diameter was applied *via* photolithography and with an Ar-ion beam the unwanted parts of the GDC20 film were removed (a micrograph of the resulting structure is depicted in Fig. 3 a). For sample type 2, a plain GDC20 thin film was deposited by PLD on a YSZ substrate in the first step. In the next step, a droplet of a slurry – consisting of Al_2O_3 particles dispersed in an organic solvent (mainly terpineol) – was deposited on the GDC20 film. This procedure resulted in coverage of a nearly circular shaped area by a loosely bound Al_2O_3 compact, which acted as a mask in the subsequent Ar-ion beam treatment and prevented removal of the GDC20 film at this certain area. The GDC20 thin film was completely removed everywhere except the masked area until only YSZ as substrate material was present. The use of such a particle slurry was necessary, due to the elevated temperature during the following PLD step. Onto

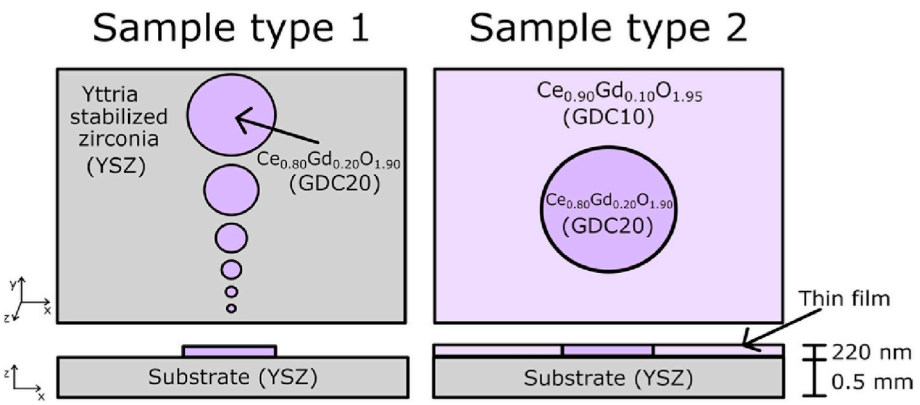

Fig. 1. Schematic illustration of structured sample design.

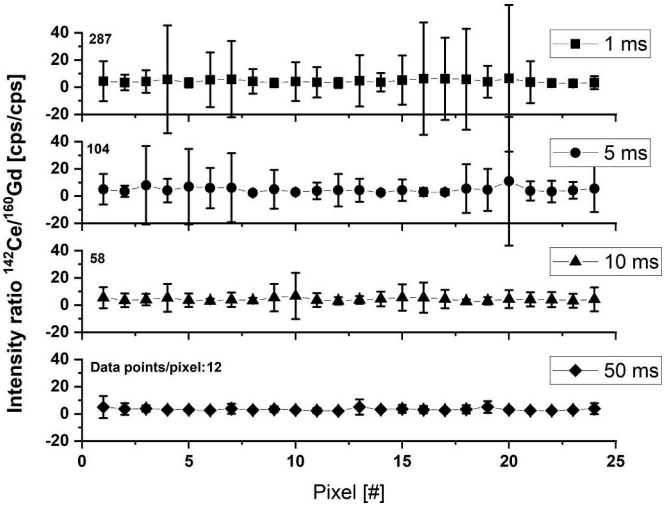

Fig. 2. Influence of the dwell time on the variance of $^{142}Ce/^{160}Gd$ ratio when ablating a homogeneous GDC10 thin film and applying the same data processing procedure as for image calculation. Longer dwell times show much smaller standard deviation, due to much less variances of the single datapoints of one pixel.

the free YSZ surface, which surrounds the masked region, a thin film of GDC10 was deposited and the Al_2O_3 compact avoids deposition of GDC10 on top of the circular GDC20 structure. After GDC10 deposition, the Al_2O_3 particle deposit was simply wiped off. As a result, sample type 2 shows only one GDC20 circle surrounded by GDC10. In Fig. 5 a) an optical micrograph of the prepared sample is depicted. Due to the different preparation process, the edge of the GDC20 circle in sample type 2 is not as sharp as the edge of the circles in sample type 1. Both thin films of sample type 2 are in direct contact with the bare substrate, have the same thickness and owing to the relatively low deposition temperature the two different dopant levels of the cerium oxide cannot be intermixed with each other.

2.3. Online-LASIL sampling

After placing the sample in the cavity of the ablation cell body and fixing the cover glass with screws and a metal ring, the whole cell is mounted on the moveable sample stage of the ablation instrument. For particle transport, diluted hydrochloric acid (1% v/v) obtained by mixing concentrated hydrochloric acid (37 mass%, EMSURE®, Merck, Germany) with deionised water provided by Barnstead™ Easypure™ II

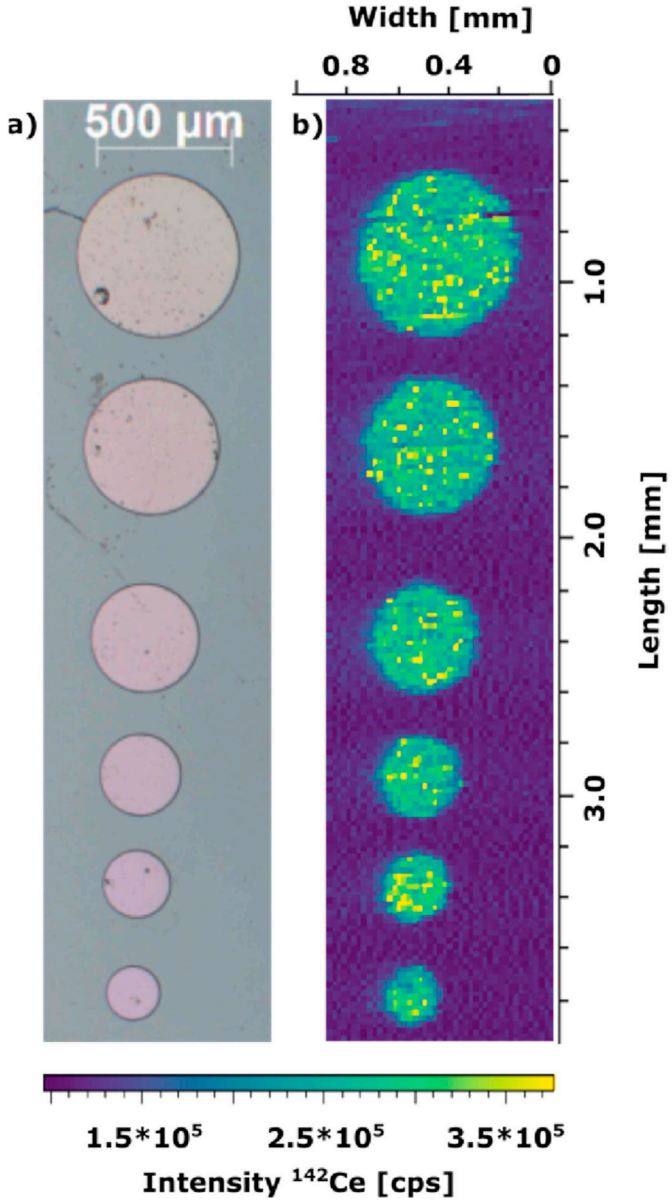

Fig. 3. a) Optical microscope image of the structured sample of sample type 1 and b) raw intensity map of ^{140}Ce to show the imaging possibility with this online-LASIL technique.

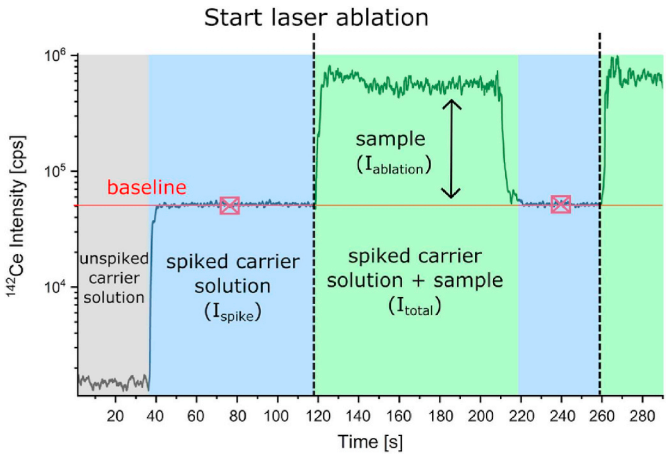

Fig. 4. Adapted diagram of online-quantification approach with a modified standard addition concept. Carrier solution with a known amount of analytes is "spiked" by sample particles produced in laser ablation process. Sample concentration is calculated by using the baseline of the spiked carrier solution offering a fast method for signal quantification.

(18.2 MΩ cm^{-1}) was used. Furthermore, certain amounts of single element liquid standards of Ce (Specpure®, Alfa Aesar, ThermoFisher, Germany) and Gd (Certipure®, Merck, Germany) were added. The resulting analyte concentration in the carrier solution (2.5 µg g^{-1} Ce, 1.0 µg g^{-1} Gd) is used later on for signal quantification. Flowrate of the carrier solution is 0.6 mL min^{-1} and the carrier flow is segmented by air bubbles introduced by a T-piece. As demonstrated in our previous work [20], the segmentation is beneficial for a fast particle washout from the ablation cell and prevents particle dispersion during the transportation.

Laser ablation parameters were chosen to achieve complete ablation of the GDC thin film, sufficient signal intensity for the detection system and high lateral resolution. The smallest laser spot, which still allows detection of the ablated particles, was 10 µm. Though 10 µm spot size offers higher lateral resolution than 20–25 µm, the bigger spot sizes were favoured due to a significantly improved signal/noise ratio resulting in a better image quality according to the findings of van Elteren et al. [21]. Parallel adjoining line scans were performed to ablate the sample area of interest. For further details on ablation parameters see Table 1. After signal quantification in OriginPro 2019-software (version 9.6.5.169, OriginLab Cooperation), the images were reconstructed using ImageLab-software (verison 2.99, Epina GmbH, Retz, Austria).

A careful choice of the appropriate isotopes for the determination of Gd and Ce with ICP-MS is important, to avoid isobaric interferences. ^{156}Gd for example should be obviated due to the risk of isobaric interferences caused by Ce (^{140}Ce + ^{16}O = ^{156}Gd). Three isotopes of each element were investigated in preliminary experiments to find the best combination of isotopes. In these experiments, ^{138}Ce and ^{155}Gd showed a poor signal/background ratio and were discarded. Quantifying the remaining two isotopes per element with a liquid standard revealed no significant difference between the results of the two isotopes of one element. For imaging experiments ^{142}Ce and ^{160}Gd were used, due to their higher abundance and/or better signal/background ratio compared to the other isotopes.

3. Results and discussion

3.1. Dwell time optimisation

In quadrupole-based mass spectrometers all elements are sequentially analysed. The time spent on recording one $\frac{m}{z}$-value is called dwell time. During this time period, all incoming ions of only one $\frac{m}{z}$-value are detected, all the other ions are discarded. For the measurement of steady state signals – for example when measuring liquid samples – this type of analyser is well feasible. However, if it comes to transient signals, one might run into the difficulty to monitor fast signal changes of multiple ions. In order to optimise this parameter, one has to find a compromise between two conflictive interests: (i) good counting statistics and (ii) enough data points for fast transient signals.

If such fast transient signals are expected (which is especially the case for imaging experiments) and more than one $\frac{m}{z}$-value is of interest, the sum of all dwell times needs to be much shorter than the duration of the transient signal, to be able to resolve the trend of the transient signal for each species of interest [22]. If short dwell times are applied, the signal intensity has to be high, otherwise the relative statistical error (RSE) will rise due to poor counting statistics [23]. This fact is especially important for precise isotope ratio measurements. Even though this work does not focus on determining isotope ratios but on obtaining elemental ratios (e.g. Gd/Ce), attention has to be drawn onto such data acquisition parameters to minimize systematic errors due to improper dwell times. In our specific case the signal intensities for ^{142}Ce range between 50 000–600 000 cps and 40 000–200 000 cps for ^{160}Gd, which are quite moderate values, all detectable in the counting mode of the detector and thereby avoiding the necessity to change the detector mode to analog, which is also known to be disadvantageous [24]. The second property, which has to be considered when optimizing the dwell time, is the variability of the transient signals. The maximum variability can be deduced by the washout time of the ablation cell. For the

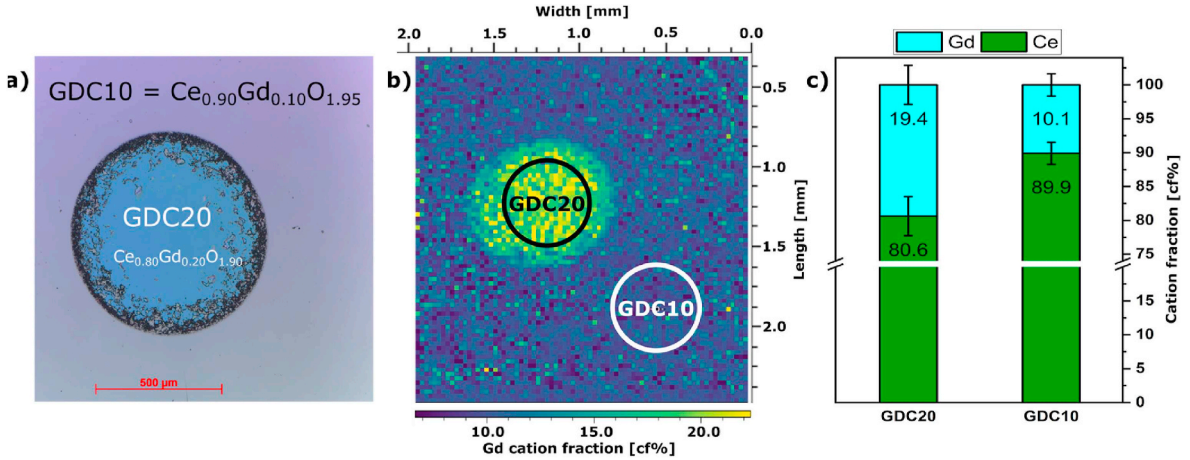

Fig. 5. a) Optical microscope picture of sample type 2, b) quantified online-LASIL image of the same sample and c) pixel average of the two different GDC types with their corresponding standard deviation (1 s, n = 300) marked with two circles in part b).

ablation cell used in the present study the washout time ($FW_{0.01}$) was determined to be 5.0 ± 0.6 s (n = 24, +/− 1σ). Compared to conventional laser ablation with He or Ar as transportation gas, where washout times are usually below 0.5 s for commercially available LA-systems and sometimes even less than 10 ms for custom made ablation cells [25], the washout time of the online-LASIL cell is fairly long. Owing to the counting statistics of our analytes and the long duration of the transient signal, rather long dwell times are preferable, since the risk of recording a too little number of data points appears to be negligible.

To systematically investigate the influence of the dwell time on the results for the given samples and certain online-LASIL setup, additional experiments were carried out. Eight lines – with a length of 600 µm each – were ablated from a homogeneous GDC10 thin film with the parameters given in Table 1. Solely the dwell time was varied from 1 to 50 ms with a certain dwell time being used for each ablation line. Subsequently, the ratio of the signal intensities of the two elements Gd and Ce was calculated for each data point. With the ablation parameters given in Table 1, the ablated line would represent 24 pixels in an image. Consequently, for the shortest dwell time 287 and for the longest 12 data points were averaged per pixel. In Fig. 2 average value and the corresponding single standard deviation of the 24 pixels are depicted for four representative dwell times. For very short dwell times the variance of the data points combined to one pixel is very high resulting in large standard deviations. For longer dwell times – such as 20, 30 or 50 ms – the standard deviation gets much smaller although the number of data points combined in one pixel is decreasing. These findings confirm the considerations mentioned above, that for the present case a relatively long dwell time is feasible and even preferable to improve the obtained data quality. For that reason 50 ms dwell time were selected for all further experiments.

3.2. Online-LASIL 2D intensity maps

The design of our online-LASIL ablation cell gives the unique opportunity to correlate the analyte signal with the ablation spot due to the constant particle transport by the carrier solution. All other LASIL setups presented in literature so far use some container filled with a stationary liquid [13,14,26]. Although the ablation spot may not be stationary in these studies, the particles from different ablation sites are all suspended in the same liquid. The subsequent analysis of this suspension delivers averaged bulk information only, despite possible lateral variations of the sample.

To indeed prove the possibility of differentiating particles from different ablation sites with our online-LASIL cell, a structured GDC thin film of sample type 1 was analysed. With this sample type the question about the area of origin of the particles can be easily answered, because in certain areas – i.e. the violet circles in Fig. 1 – Gd and Ce are present, while in areas surrounding the circles this is not the case. Owing to the characteristic structure of the patterned GDC films, it easily possible to judge whether the correlation of the particle's origin is correct or not. Therefore, an optical microscope image and the intensity map of ^{142}Ce are compared in Fig. 3. In this 2D intensity map, the six GDC circles (in green to yellow) can be clearly distinguished from the bare substrate (in blue). The size of the circles in the microscope image ranges from 600 µm to 150 µm and even the smallest circle is clearly visible in the LASIL image, thus demonstrating a good lateral resolution. The size of the ablated area was about 3.5 × 0.9 mm^2 and the complete measurement took about 3 h. Compared to conventional LA measurements with He or Ar as ablation and transport gas the measurement time is about 3 or more times larger. However, one has to keep in mind, that for conventional LA-experiments, several 100 mL min^{-1} of He or Ar are used for particle transport, while in the case of online-LASIL, much smaller flow rates of an aqueous medium of about 0.6 mL^{-1} are applied. Furthermore, this is the first time that this online-LASIL technique was used for recording 2D intensity maps and several future improvements are expected, which will significantly speed up the imaging process.

3.3. Online standard addition quantification strategy

Qualitative information as presented in the previous section is already very useful, for example when comparing two different positions in one sample. However, quantitative data is of even more interest and therefore required. LASIL sampling offers the opportunity to achieve this goal without solid reference materials, which is a major advantage of this technique.

Quantification of nanoparticle suspensions with liquid reference materials – as it was applied herein – has been investigated several times confirming its applicability. Ebdon et al. [27,28] and Chen et al. [29] have performed fundamental studies on slurries and reported that for ICP-based analysis methods suspensions with particles smaller than 2.5 µm [27] or 5 µm [29] and below a certain concentration level can practically be treated like solutions. Nowadays this concept is applied to several fields of analytical chemistry like single particle ICP-MS [30] or LASIL-ICP-MS. There are various reports of suspensions specifically produced by LASIL of different materials (glass [14,15], metals [13], ceramics [16,17,26,31]) which were quantified by liquid standards proving the applicability and reporting particle sizes usually smaller than 100 nm.

Preliminary experiments were performed with a particle tracking analyser (ZetaView®, Particle Metrix, Germany). The size distribution of the particles produced with our current online-LASIL ablation setup ranges from 80 nm to 200 nm with the maximum number of the particles having a size of 100 nm. Given this particle size distribution and a fairly low particle concentration, all requirements for a correct quantification with liquid standard solutions are met.

In our previous work, sequential measurement of standard and sample in bracketing mode was used for signal quantification to obtain very precise results [20]. This approach has many benefits, especially when used for the measurement of bulk samples, because there is only a very short time between standards and sample. However, for imaging experiments this approach is hardly feasible due to practical problems: (i) Either the standards are measured only once before and after the whole imaging experiment, which might work out for very small images of only a few minutes of measurement time. For rather long imaging experiments of several hours, accuracy will suffer due to instrumental drifts (e.g. variations in nebulizer efficiency) if the standards are measured only once before and after data recording. (ii) The standards are measured before and after each ablation line. This approach, however, is also practically unfeasible, if there is no automated system available that manages changing from plain carrier solution to standard solution.

To avoid potential problems associated with possible changes in instrumental conditions between sample and standard we adapted the standard addition concept. For this reason, the carrier solution was spiked with known amounts of liquid standard solutions. This spiked carrier solution transports the particles produced during the ablation process to the detection system and serves as a standard in the same measurement, when no particles are ablated, resulting in an online-measurement of sample and standard. Thereby the measurement time can be reduced and no manual or automated change of the carrier solution is necessary.

The measured total analyte intensity I_{total} during this ablation process is determined by the known spike concentration I_{spike} and the unknown amount of ablated material $I_{ablation}$ and is given by equation (1):

$$I_{total} = I_{spike} + I_{ablation} \quad (1)$$

In Fig. 4 there is a visualisation of the different intensity levels: unspiked carrier solution (blank), spiked carrier solution (I_{spike}), and spiked carrier solution plus sample (I_{total}). Since the signal intensity caused by the spike can be mathematically interpolated over the period of ablation, it is possible to calculate the contribution of the ablated

particles to the total signal intensity. When using the information about the analyte concentration in the carrier solution c_{spike}, the signal intensity caused by the spike I_{spike} and the total intensity I_{total}, the analyte concentration of the ablated material $c_{ablation}$ can be obtained by:

$$c_{ablation} = \frac{c_{spike}}{I_{spike}} * (I_{total} - I_{spike}) \quad (2)$$

The calculated concentrations of both analytes (this case Gd, Ce) obtained by eq. (2) are then converted into molar concentrations using the molar weight of each element. Based on these values the cation sample composition in units of cation fraction cf% is calculated by eq. 3:

$$fraction_{analyte\ 1} = \frac{c'_{analyte\ 1}}{c'_{analyte\ 1} + c'_{analyte\ 2}} * 100$$

where $c'_{analyte}$ is the concentration in μmol g^{-1} measured for the analyte in the nanoparticle suspension generated in the LASIL process.

As depicted in Fig. 4 after each ablation line the signal intensity drops back to the baseline for a certain amount of time before the next ablation line starts. For a mathematical interpolation, at least two interpolation points are necessary resulting in a linear regression. If there are changes of the baseline, for example due to instrumental drifts over a long period of measurement, or due to some particle dispersion in the system after the very first ablation lines, these changes can be corrected by adapting and adding interpolation points. Thus, this kind of quantification approach is very flexible, since it is possible to set interpolation points after every ablation line. This is equal to measuring a separate standard solution before and after each line, but much more time effective. Furthermore, the quantification of nanoparticles produced by LASIL with liquid standard solution offers a high flexibility concerning the concentration range and the elements of interest in the sample, since the commercially available liquid reference material can be easily mixed and diluted.

3.4. Quantified online-LASIL images

As the easy quantification with liquid standards is a major advantage of this LASIL sampling strategy, we also wanted to demonstrate the quantification capabilities in combination with the imaging possibilities. For this purpose, a GDC thin film of sample type 2 was analysed. This sample type was designed to have two distinguishable areas with slightly different chemical compositions, thus demonstrating the simultaneous correlation of the signal to the correct ablation area together with a correct quantification by using liquid standards. Fig. 5 a) depicts an optical micrograph to visualise the actual sample before ablation. The GDC20 circle has a diameter of 775 μm. Fig. 5 b) shows the reconstructed image after ablation of the sample. It is important to point out that the colour scale of the image gives already quantified information, not just raw intensities. This means, that a yellow colour represents higher Gd content and blue lower Gd content. With this colour scale, the circle containing GDC20 is clearly distinguishable from the surrounding GDC10 thin film. Whether the calculated composition is correct, can be checked in part c) of Fig. 5. Therefore, the encircled pixels are averaged (n = 300) and the results are depicted as a bar diagram. Pixels at the edge of the GDC20 circle are omitted, to avoid an influence of the GDC10 surrounding thin film. The average of the pixels in the area of the GDC20 circle (yellow area in Fig. 5 b) is 19.4 ± 2.8 cf % (1s, n = 300) for Gd and 80.6 ± 2.8 cf% (1s, n = 300) for Ce, which is in very good agreement with the nominal composition provided by the supplier of the PLD target (20 cf% Gd. 80 cf% Ce). Furthermore, unstructured thin films of this material have been previously investigated by online-LASIL-ICP-OES (i.e. without imaging) [20]. The measured composition given in this publication (21.9 ± 0.3 cf% for Gd, 78.1 ± 0.3 cf% for Ce) also confirms the value found for the GDC20 circle within the online-LASIL-ICP-MS imaging experiment. The results of the GDC10 area (10.1 ± 1.6 cf% Gd, 89.9 ± 1.6 cf% Ce) are also in excellent agreement with the nominal value of the material.

The difference in the variances of both measurements (online-LASIL-ICP-OES or –MS measurement) are close to a factor of 10. This can be explained by the different size of the sampled area. For one online-LASIL-ICP-OES measurement an area of 1.9 mm^2 was ablated, analysed, and averaged. For one pixel of the online-LASIL-ICP-MS measurement only $4.9*10^{-4}$ mm^2 were ablated. The significantly lower absolute amount of ablated material requires the use of an ICP-MS instrument for analysis and increases the variance. Nevertheless, the variance of the online-LASIL-ICP-MS measurement is absolutely comparable to variances of conventional LA-ICP-MS measurements if quantified with solid reference materials [32].

4. Conclusion

The focus of this work is to demonstrate the 2D imaging potential of the online-LASIL sampling strategy. For this purpose, an in-house built online-LASIL ablation cell was designed and optimized, which is directly coupled with a detection system. The nanoparticles produced in the ablation process are constantly transported to the liquid sample introduction system by an aqueous carrier solution. Due to this unique feature of the online-LASIL system, we are able to correlate the measured signal intensities with the spatial origin of the particles. To illustrate the 2D imaging capability of our online-LASIL system, two types of geometrically structured thin film samples were prepared by pulsed laser deposition and ion beam etching procedures. To the best of our knowledge, the reconstructed images are the first reported images obtained by online-LASIL and show good lateral resolution, especially when compared to the first publications of conventional LA-ICP-MS images [33].

Furthermore, with an adapted online standard addition quantification strategy we were able to correctly quantify the cation composition of a Gd-doped ceria thin film of 220 nm thickness. This online quantification approach is a fast alternative especially for long measurement times (e.g. imaging), because sample and standard are not measured subsequently, but almost simultaneously and the liquid standards turned out to be once more a major advantage of the LASIL sampling strategy.

CRediT authorship contribution statement

C. Herzig: Investigation, Writing - original draft. **J. Frank:** Resources. **A.K. Opitz:** Conceptualization. **J. Fleig:** Conceptualization. **A. Limbeck:** Conceptualization, Methodology, Supervision, Funding acquisition.

Declaration of competing interest

The authors declare that they have no known competing financial interests or personal relationships that could have appeared to influence the work reported in this paper.

Acknowledgement

The authors gratefully thank the FWF Austrian Science Fund for supporting this project number P31165–N37.

References

[1] J. Neddersen, G. Chumanov, T.M. Cotton, Appl. Spectrosc. 47 (1993) 1959–1964.
[2] T.T.P. Nguyen, R. Tanabe-Yamagishi, Y. Ito, Appl. Surf. Sci. 470 (2019) 250–258.
[3] T.T.P. Nguyen, R. Tanabe, Y. Ito, Optic Laser. Technol. 100 (2018) 21–26.
[4] J. Tomko, S.M. O'Malley, C. Trout, J.J. Naddeo, R. Jimenez, J.C. Griepenburg, W. Soliman, D.M. Bubb, Colloid. Surface. Physicochem. Eng. Aspect. 522 (2017) 368–372.
[5] G.W. Yang, Prog. Mater. Sci. 52 (2007) 648–698.

[6] F. Mafuné, J.-y. Kohno, Y. Takeda, T. Kondow, J. Phys. Chem. B 106 (2002) 7575–7577.
[7] R. Intartaglia, K. Bagga, F. Brandi, G. Das, A. Genovese, E. Di Fabrizio, A. Diaspro, J. Phys. Chem. C 115 (2011) 5102–5107.
[8] N.G. Semaltianos, S. Logothetidis, W. Perrie, S. Romani, R.J. Potter, M. Sharp, P. French, G. Dearden, K.G. Watkins, Appl. Phys. A 94 (2008) 641.
[9] C.L. Sajti, R. Sattari, B.N. Chichkov, S. Barcikowski, J. Phys. Chem. C 114 (2010) 2421–2427.
[10] K.Y. Niu, J. Yang, S.A. Kulinich, J. Sun, X.W. Du, Langmuir 26 (2010) 16652–16657.
[11] M.K. Singh, M.C. Mathpal, A. Agarwal, Chem. Phys. Lett. 536 (2012) 87–91.
[12] S. Yang, W. Cai, H. Zeng, X. Xu, J. Mater. Chem. 19 (2009) 7119–7123.
[13] E.V. Muravitskaya, V.A. Rosantsev, M.V. Belkov, E.A. Ershov-Pavlov, E.V. Klyachkovskaya, Spectrochim. Acta B Atom Spectrosc. 64 (2009) 119–125.
[14] D.N. Douglas, J.L. Crisp, H.J. Reid, B.L. Sharp, J. Anal. Atom. Spectrom. 26 (2011) 1294–1301.
[15] S. Okabayashi, T.D. Yokoyama, Y. Kon, S. Yamamoto, T. Yokoyama, T. Hirata, J. Anal. Atom. Spectrom. 26 (2011) 1393–1400.
[16] R. Machida, R. Nishioka, M. Fujiwara, N. Furuta, Anal. Sci. 33 (2017) 537–544.
[17] K. Hirosawa, N. Furuta, Anal. Sci. 35 (2019) 557–563.
[18] A. Limbeck, M. Bonta, W. Nischkauer, J. Anal. Atom. Spectrom. 32 (2017) 212–232.
[19] M. Bonta, J. Frank, S. Taibl, J. Fleig, A. Limbeck, Anal. Chim. Acta 1000 (2018) 93–99.
[20] C. Herzig, J. Frank, A.K. Opitz, J. Fleig, A. Limbeck, J. Anal. Atom. Spectrom. 34 (2019) 2333–2339.
[21] J.T. van Elteren, M. Šala, V.S. Šelih, Anal. Chem. 90 (2018) 5916–5922.
[22] H.J. Landau, Proc. IEEE 55 (1967) 1701–1706.
[23] D.R. Bandura, S.D. Tanner, Atom. Spectros 20 (1999) 69–72.
[24] M.E. Kylander, D.J. Weiss, T.E. Jeffries, B. Kober, A. Dolgopolova, R. Garcia-Sanchez, B.J. Coles, Anal. Chim. Acta 582 (2007) 116–124.
[25] S.J.M. Van Malderen, A.J. Managh, B.L. Sharp, F. Vanhaecke, J. Anal. Atom. Spectrom. 31 (2016) 423–439.
[26] M. Fujiwara, K. Hirosawa, N. Nonose, S. Nishida, N. Furuta, Accred Qual. Assur. (2019), https://doi.org/10.1007/s00769-019-01389-5.
[27] L. Ebdon, M.E. Foulkes, S. Hill, J. Anal. Atom. Spectrom. 5 (1990) 67–73.
[28] L.E.S. Ebdon, M. Foulkes, K. Sutton, J. Anal. Atom. Spectrom. 12 (1997) 213–229.
[29] C. Chen, T.W. McCreary, Appl. Spectrosc. 48 (1994) 410–412.
[30] H.E. Pace, N.J. Rogers, C. Jarolimek, V.A. Coleman, C.P. Higgins, J.F. Ranville, Anal. Chem. 83 (2011) 9361–9369.
[31] R. Machida, T. Nakazawa, Y. Sakuraba, M. Fujiwara, N. Furuta, J. Anal. Atom. Spectrom. 30 (2015) 2412–2419.
[32] A. Limbeck, P. Galler, M. Bonta, G. Bauer, W. Nischkauer, F. Vanhaecke, Anal. Bioanal. Chem. 407 (2015) 6593–6617.
[33] J.S. Becker, M.V. Zoriy, C. Pickhardt, N. Palomero-Gallagher, K. Zilles, Anal. Chem. 77 (2005) 3208–3216.